

# Constraints on the anomalous Higgs boson couplings in $Z\gamma\gamma$ production at muon collider

S. Spor<sup>1,\*</sup>

<sup>1</sup>*Department of Medical Imaging Techniques,  
Zonguldak Bülent Ecevit University, 67100, Zonguldak, Türkiye.*

## Abstract

We investigate the sensitivities on the Wilson coefficients of dimension-six operators associated with the anomalous  $H\gamma\gamma$ ,  $H\gamma Z$  and  $HZZ$  vertices through the process  $\mu^-\mu^+ \rightarrow Z\gamma\gamma$  at future muon collider. Signal events involving Higgs-gauge boson interactions and relevant backgrounds events at the muon collider designed with center-of-mass energy of 10 TeV and integrated luminosity of  $10 \text{ ab}^{-1}$  are generated in Madgraph within the framework of the model-independent Standard Model effective field theory and detector effects are also included with corresponding detector cards in Delphes. The limits at 95% C.L. on the coefficients  $\bar{c}_{HB}$  and  $\bar{c}_{HW}$  are reported to be  $[-0.0052; 0.0040]$  and  $[-0.0034; 0.0023]$ , respectively, and compared with the experimental and phenomenological limits.

---

\*serdar.spor@beun.edu.tr

## I. INTRODUCTION

With the discovery of the Higgs particle [1, 2], intensive studies have been done to reveal the properties of the Higgs particle at colliders, both through the Standard Model (SM) predictions and scenarios beyond the SM. Despite the discovery of the Higgs boson, the Higgs sector's structure is still unclear. Despite many successful predictions of the SM, its clear discrepancies with some experimental observations and its inability to explain some major problems such as dark matter, dark energy, hierarchy problem, strong CP problem, etc. encourage us to search for indirect signatures of new physics.

New physics extensions beyond the SM are necessary to address unresolved open questions like the observed baryon-antibaryon asymmetry of the Universe, even if studies [3–7] indicate that the currently discovered Higgs boson is a CP-even scalar with CP-conserving interactions and is in accord with the SM predictions. In cosmology and particle physics, one of the biggest puzzles is the Baryon Asymmetry of the Universe (BAU). If three Sakharov conditions [8] are met, the mechanism of electroweak baryogenesis (EWBG) [9] can explain the matter-antimatter asymmetry. These conditions are: (i) baryon number violation, (ii) C and CP violation, and (iii) deviation from the thermodynamic equilibrium.

The quantity of CP violation in the SM caused by the Cabibbo-Kobayashi-Maskawa (CKM) matrix [10, 11] is insufficient to quantitatively reproduce the BAU [12, 13] if we concentrate on the second of these three conditions. Extended Higgs sectors that offer more sources of CP violation can solve this issue. In particle physics, one crucial area of study for future experiments is the search for CP violation. One of the prerequisites for baryogenesis is CP violation, and quark flavor physics which is in accord with the CKM mechanism in the SM [11] provides the only experimental proof of CP violation to date. Therefore, an intriguing way to search for a new mechanism is to look for CP violation in the interactions between the Higgs boson and gauge bosons. A major goal of experimental measurements is to restrict the certain range of CP-violating parameters or to find nonzero CP violation in the Higgs boson interactions. Future high-energy physics experiments have special qualifications to test for CP violation in the Higgs boson interactions. Since CP violation impacts are negligible in the SM, they offer great testing opportunities to compare the performance of future facilities. The studies of Higgs boson phenomenology have come into prominence in searching for the SM and new physics effects at current and future

colliders. The search for precise measurements of Higgs boson couplings at multi-TeV muon colliders has recently become more important in the study of physics beyond the SM [14–28]. The presence of theories beyond the SM that can predict effects of CP violation will have significant outcomes for particle physics in the future.

## II. EFFECTIVE OPERATORS AND HIGGS-GAUGE BOSON INTERACTIONS

A new physics model with additional fields and interactions is needed to make progress in particle physics. In order to understand the new physics in light of experimental data, it is necessary to establish the relationship between the observables at the electroweak scale and physics beyond the SM at a relatively high scale. In order to describe new physics at high mass scales, effective field theory (EFT) presents a model-independent way. EFTs are a tool to bridge the gap between scales and reveal the indirect the new physics effects from experimental data.

The EFT is only valid up to a particular energy scale ( $\Lambda$ ); in order for the theory to be practical, it must be above the energy scale ( $E$ ) that is immediately accessible experimentally. In other words, when  $\Lambda \gg E$ , the EFT gives a good approximation. In the EFT framework, the effects of unobserved states, which are predicted to arise at energies bigger than an effective scale determined by the  $W$ -boson mass  $m_W$ , are parameterized using high-dimensional operators for interactions beyond the SM.

One of the most effective ways to measure the effects of the new physics is to use higher-dimensional effective operators consisting of SM fields that obey the SM gauge symmetry. These are named the Standard Model Effective Field Theory (SMEFT) operators. In this approximation, additional dimension-six operators are added to the SM Lagrangian to ensure conservation of lepton and baryon numbers, and dimension-eight and higher operators are neglected for further suppression. The SMEFT operators can be expressed in a theoretical context in the Strongly Interacting Light Higgs (SILH) basis.

An effective theory of a light composite Higgs boson, which is responsible for the electroweak symmetry breaking and arises as the pseudo-Goldstone boson from a strongly interacting sector, reveals the SILH basis [29]. The effective Lagrangian of the  $H\gamma\gamma$ ,  $HZZ$  and  $H\gamma Z$  couplings in the SILH basis [30] is described as the sum of the Lagrangian involving the CP-conserving and CP-violating dimension-six operators and the dimension-four SM

Lagrangian as follows:

$$\mathcal{L} = \mathcal{L}_{\text{SM}} + \sum_i \bar{c}_i \mathcal{O}_i = \mathcal{L}_{\text{SM}} + \mathcal{L}_{\text{CPC}} + \mathcal{L}_{\text{CPV}} \quad (1)$$

where  $\bar{c}_i$  are the Wilson coefficients normalized with the new physics scale  $\Lambda$  determined by the  $W$ -boson mass  $m_W$  and  $\mathcal{O}_i$  are the dimension-six operators. The effective Lagrangian with the CP-conserving and CP-violating operators corresponding to the second and third terms in Eq. (1), respectively, are shown below [31]

$$\begin{aligned} \mathcal{L}_{\text{CPC}} = & \frac{\bar{c}_H}{2v^2} \partial^\mu (\Phi^\dagger \Phi) \partial_\mu (\Phi^\dagger \Phi) + \frac{\bar{c}_T}{2v^2} (\Phi^\dagger \overleftrightarrow{D}^\mu \Phi) (\Phi^\dagger \overleftrightarrow{D}_\mu \Phi) \\ & + \frac{ig\bar{c}_W}{m_W^2} (\Phi^\dagger T_{2k} \overleftrightarrow{D}^\mu \Phi) D^\nu W_{\mu\nu}^k + \frac{ig'\bar{c}_B}{2m_W^2} (\Phi^\dagger \overleftrightarrow{D}^\mu \Phi) \partial^\nu B_{\mu\nu} \\ & + \frac{2ig\bar{c}_{HW}}{m_W^2} (D^\mu \Phi^\dagger T_{2k} D^\nu \Phi) W_{\mu\nu}^k + \frac{ig'\bar{c}_{HB}}{m_W^2} (D^\mu \Phi^\dagger D^\nu \Phi) B_{\mu\nu} \\ & + \frac{g'^2 \bar{c}_\gamma}{m_W^2} \Phi^\dagger \Phi B_{\mu\nu} B^{\mu\nu} \end{aligned} \quad (2)$$

and

$$\mathcal{L}_{\text{CPV}} = \frac{ig\tilde{c}_{HW}}{m_W^2} D^\mu \Phi^\dagger T_{2k} D^\nu \Phi \tilde{W}_{\mu\nu}^k + \frac{ig'\tilde{c}_{HB}}{m_W^2} D^\mu \Phi^\dagger D^\nu \Phi \tilde{B}_{\mu\nu} + \frac{g'^2 \tilde{c}_\gamma}{m_W^2} \Phi^\dagger \Phi B_{\mu\nu} \tilde{B}^{\mu\nu} \quad (3)$$

where  $v$  is the vacuum expectation value of the Higgs field.  $\tilde{B}_{\mu\nu} = \frac{1}{2}\epsilon_{\mu\nu\rho\sigma} B^{\rho\sigma}$  and  $\tilde{W}_{\mu\nu}^k = \frac{1}{2}\epsilon_{\mu\nu\rho\sigma} W^{\rho\sigma k}$  are the dual field strength tensors defined by the field strength tensors  $B_{\mu\nu} = \partial_\mu B_\nu - \partial_\nu B_\mu$  and  $W_{\mu\nu}^k = \partial_\mu W_\nu^k - \partial_\nu W_\mu^k + g\epsilon_{ij}^k W_\mu^i W_\nu^j$  with gauge couplings  $g'$  and  $g$ . The  $SU(2)_L$  generators are written as  $T_{2k} = \sigma_k/2$ , where  $\sigma_k$  is the Pauli matrices.  $D^\mu$  is covariant derivative operator with  $\Phi^\dagger \overleftrightarrow{D}_\mu \Phi = \Phi^\dagger (D_\mu \Phi) - (D_\mu \Phi^\dagger) \Phi$ , where  $\Phi$  is the Higgs doublet in SM. In the unitarity gauge and mass basis, the Lagrangian with triple interaction terms with the Higgs sector for the  $H\gamma\gamma$ ,  $H\gamma Z$  and  $HZZ$  couplings is given below [31]:

$$\begin{aligned} \mathcal{L} = & -\frac{1}{4}g_{h\gamma\gamma} F_{\mu\nu} F^{\mu\nu} h - \frac{1}{4}\tilde{g}_{h\gamma\gamma} F_{\mu\nu} \tilde{F}^{\mu\nu} h - \frac{1}{4}g_{hzz}^{(1)} Z_{\mu\nu} Z^{\mu\nu} h - g_{hzz}^{(2)} Z_\nu \partial_\mu Z^{\mu\nu} h \\ & + \frac{1}{2}g_{hzz}^{(3)} Z_\mu Z^\mu h - \frac{1}{4}\tilde{g}_{hzz} Z_{\mu\nu} \tilde{Z}^{\mu\nu} h - \frac{1}{2}g_{h\gamma z}^{(1)} Z_{\mu\nu} F^{\mu\nu} h - \frac{1}{2}\tilde{g}_{h\gamma z} Z_{\mu\nu} \tilde{F}^{\mu\nu} h - g_{h\gamma z}^{(2)} Z_\nu \partial_\mu F^{\mu\nu} h \end{aligned} \quad (4)$$

where  $h$ ,  $F_{\mu\nu}$  and  $Z_{\mu\nu}$  are the Higgs-boson field, the field strength tensors of photon and  $Z$ -boson, respectively.  $\tilde{F}^{\mu\nu} = \frac{1}{2}\epsilon^{\mu\nu\rho\sigma} F_{\rho\sigma}$  and  $\tilde{Z}^{\mu\nu} = \frac{1}{2}\epsilon^{\mu\nu\rho\sigma} Z_{\rho\sigma}$  are the dual field strength

tensors. The relationships among the Lagrangian parameters in the mass basis in Eq. (4) and the gauge basis in Eqs. (2-3) are shown below:

$$\tilde{g}_{h\gamma\gamma} = -\frac{8g\tilde{c}_\gamma s_W^2}{m_W} \quad (5)$$

$$\tilde{g}_{h\gamma z} = \frac{gs_W}{c_W m_W} [\tilde{c}_{HW} - \tilde{c}_{HB} + 8\tilde{c}_\gamma s_W^2] \quad (6)$$

$$\tilde{g}_{hzz} = \frac{2g}{c_W^2 m_W} [\tilde{c}_{HB} s_W^2 - 4\tilde{c}_\gamma s_W^4 + c_W^2 \tilde{c}_{HW}] \quad (7)$$

for CP-violating couplings and

$$g_{h\gamma\gamma} = a_H - \frac{8g\bar{c}_\gamma s_W^2}{m_W} \quad (8)$$

$$g_{h\gamma z}^{(1)} = \frac{gs_W}{c_W m_W} [\bar{c}_{HW} - \bar{c}_{HB} + 8\bar{c}_\gamma s_W^2] \quad (9)$$

$$g_{h\gamma z}^{(2)} = \frac{gs_W}{c_W m_W} [\bar{c}_{HW} - \bar{c}_{HB} - \bar{c}_B + \bar{c}_W] \quad (10)$$

$$g_{hzz}^{(1)} = \frac{2g}{c_W^2 m_W} [\bar{c}_{HB} s_W^2 - 4\bar{c}_\gamma s_W^4 + c_W^2 \bar{c}_{HW}] \quad (11)$$

$$g_{hzz}^{(2)} = \frac{g}{c_W^2 m_W} [(\bar{c}_{HW} + \bar{c}_W)c_W^2 + (\bar{c}_B + \bar{c}_{HB})s_W^2] \quad (12)$$

$$g_{hzz}^{(3)} = \frac{gm_W}{c_W^2} \left[ 1 - \frac{1}{2}\bar{c}_H - 2\bar{c}_T + 8\bar{c}_\gamma \frac{s_W^4}{c_W^2} \right] \quad (13)$$

for CP-conserving couplings. Here,  $a_H$  represents the SM contribution at the Higgs boson to two photons vertex,  $c_W = \cos\theta_W$ ,  $s_W = \sin\theta_W$  and  $\theta_W$  is the weak mixing angle.

As seen in Eqs. (5-13), the Higgs-electroweak gauge boson couplings in the effective Lagrangian in the mass basis for the anomalous  $H\gamma\gamma$ ,  $HZZ$  and  $H\gamma Z$  couplings are sensitive to the ten Wilson coefficients related to the Higgs-gauge boson couplings. These coefficients  $\bar{c}_\gamma$ ,  $\bar{c}_B$ ,  $\bar{c}_W$ ,  $\bar{c}_{HB}$ ,  $\bar{c}_{HW}$ ,  $\bar{c}_T$ ,  $\bar{c}_H$  associate with CP-conserving couplings and coefficients  $\tilde{c}_\gamma$ ,  $\tilde{c}_{HB}$ ,  $\tilde{c}_{HW}$  associate with CP-violating couplings.

We have performed analyses of the effects of dimension-six operators on Higgs-gauge boson couplings in MADGRAPH5\_aMC@NLO [32] based on Monte Carlo simulations using FeynRules [33]. In the Higgs effective Lagrangian model file of the FeynRules, the SILH Lagrangian is included along with the Wilson coefficients for Higgs boson interactions.

We investigate the potential of anomalous Higgs-gauge boson couplings on the process  $\mu^- \mu^+ \rightarrow Z\gamma\gamma \rightarrow \ell\ell\gamma\gamma$  at the muon collider and the sensitivity study of coefficients  $\bar{c}_\gamma$ ,  $\tilde{c}_\gamma$ ,  $\bar{c}_{HB}$ ,  $\tilde{c}_{HB}$ ,  $\bar{c}_{HW}$  and  $\tilde{c}_{HW}$  in anomalous  $H\gamma\gamma$ ,  $HZZ$  and  $H\gamma Z$  vertices. The stage of the muon collider with a center-of-mass energy of 10 TeV and an integrated luminosity of  $10 \text{ ab}^{-1}$  is considered [34]. By combining high-energy collisions in a clean experimental environment, the multi-TeV muon collider creates unique potential for Higgs studies by providing both precise measurements and high-energy reach in a single machine. Therefore, a 10+ TeV lepton collider that goes beyond the precision-energy dilemma is the ideal machine. Since electron-based colliders using current technology are unable to reach this energy scale, we are turning to muon colliders to probe this scale with leptons [35].

The Feynman diagrams of the process  $\mu^- \mu^+ \rightarrow Z\gamma\gamma$  are shown in Fig. 1. The three diagrams in the top row are pure SM background processes, while the other six diagrams present signal processes, including new physics contributions from the anomalous  $H\gamma\gamma$  (black dot),  $H\gamma Z$  (red dot) and  $HZZ$  (blue dot) vertices.

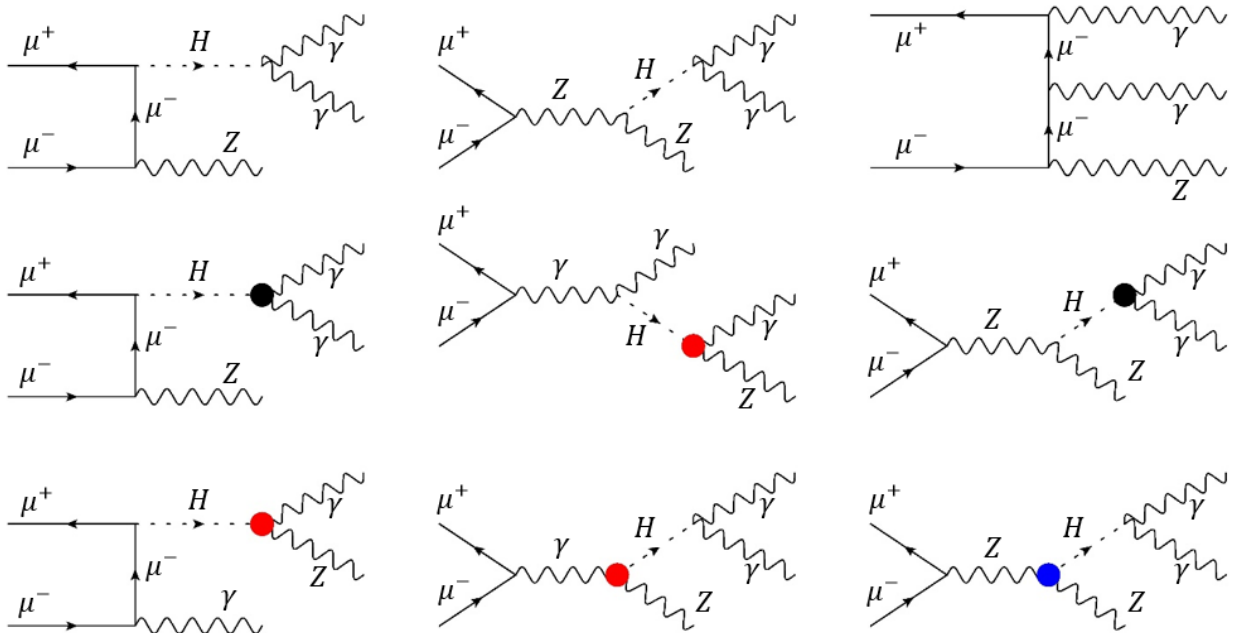


FIG. 1: The Feynman diagrams of the process  $\mu^- \mu^+ \rightarrow Z\gamma\gamma$ .

The total cross-sections of the process  $\mu^- \mu^+ \rightarrow Z\gamma\gamma$  as a function of coefficients  $\bar{c}_\gamma$ ,  $\tilde{c}_\gamma$ ,  $\bar{c}_{HB}$ ,  $\tilde{c}_{HB}$ ,  $\bar{c}_{HW}$  and  $\tilde{c}_{HW}$  at the muon collider are given in Fig. 2. The transverse momentum  $p_T^\gamma > 10$  GeV and the pseudo-rapidity  $|\eta^\gamma| < 2.5$  for the photons on the final state particles are applied to determine the total cross-sections in Fig. 2. While the other coefficients are fixed to zero, the coefficient under consideration is variable each time at the calculation method of total cross-sections. The SM cross-section including the contributions from the top three Feynman diagrams in Fig. 1 corresponds to the point  $\bar{c}_\gamma = \bar{c}_{HB} = \bar{c}_{HW} = \tilde{c}_\gamma = \tilde{c}_{HB} = \tilde{c}_{HW} = 0$  in Fig. 2.

It shows that the cross-sections as a function of the coefficients  $\bar{c}_{HB}$  and  $\bar{c}_{HW}$  are larger than those of the coefficients  $\bar{c}_\gamma$ ,  $\tilde{c}_\gamma$ ,  $\tilde{c}_{HB}$  and  $\tilde{c}_{HW}$ . That is, the process of  $Z\gamma\gamma$  production is not sensitive to changes in the coefficients  $\bar{c}_\gamma$ ,  $\tilde{c}_\gamma$ ,  $\tilde{c}_{HB}$  and  $\tilde{c}_{HW}$ , but only to  $\bar{c}_{HB}$  and  $\bar{c}_{HW}$ . Therefore, although we will present the effects of these six coefficients at the muon collider in the following sections, for the purpose of this paper we will focus on the coefficients  $\bar{c}_{HB}$  and  $\bar{c}_{HW}$ .

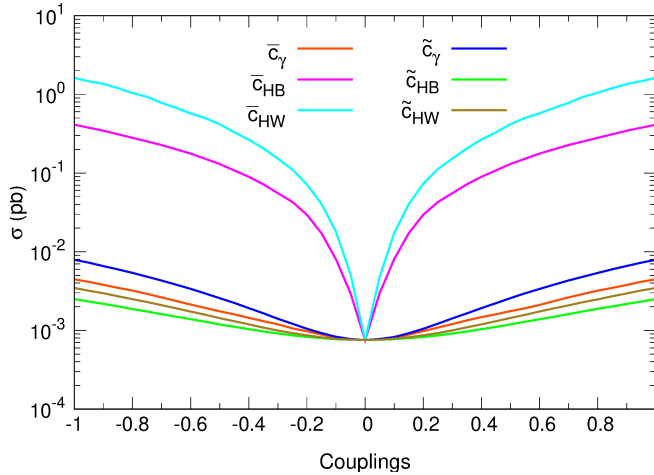


FIG. 2: The total cross-section of the process  $\mu^- \mu^+ \rightarrow Z\gamma\gamma$  as a function of coefficients  $\bar{c}_\gamma$ ,  $\tilde{c}_\gamma$ ,  $\bar{c}_{HB}$ ,  $\tilde{c}_{HB}$ ,  $\bar{c}_{HW}$  and  $\tilde{c}_{HW}$  at the muon collider.

### III. ANALYSIS OF SIGNAL AND BACKGROUND EVENTS

We describe the cut-based analysis and the detector simulation to determine the limits on anomalous Higgs-gauge boson couplings for the  $H\gamma\gamma$ ,  $HZZ$  and  $H\gamma Z$  vertices at the muon collider. The process  $\mu^- \mu^+ \rightarrow Z\gamma\gamma \rightarrow \ell\ell\gamma\gamma$  with nonzero coefficients  $\bar{c}_\gamma$ ,  $\tilde{c}_\gamma$ ,  $\bar{c}_{HB}$ ,  $\tilde{c}_{HB}$ ,  $\bar{c}_{HW}$ ,

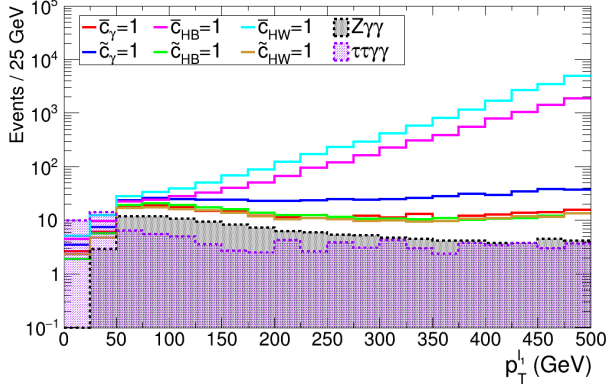
$\tilde{c}_{HW}$  is considered as signal process that comprises the SM contribution as well as interference between effective couplings and SM contributions. Two relevant backgrounds are considered; the SM contribution from the same final state of the signal process  $\mu^- \mu^+ \rightarrow Z\gamma\gamma \rightarrow \ell\ell\gamma\gamma$ , where  $\ell$  is a charged lepton such as electron ( $e^\pm$ ) and muon ( $\mu^\pm$ ), is considered as the main background process, and the process  $\mu^- \mu^+ \rightarrow \tau\tau\gamma\gamma$  is considered as the minor background process.

In MADGRAPH5\_aMC@NLO, 500k events are generated for each coefficient value of both the signal and the background processes. These events, which involve initial and final parton shower, fragmentation and decay, are processed through the Pythia 8.3 [40]. The Delphes 3.5.0 package [41] with the muon collider configuration card is used to simulate the detector responses and all events are analyzed with ROOT 6 [42].

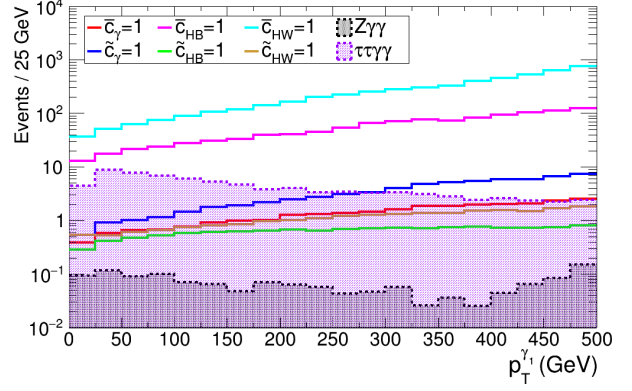
The  $\ell\ell\gamma\gamma$  channel is subjected to independent applications of the preselection and kinematic cuts in both signal and background processes to differentiate the signal from the relevant backgrounds. When identifying kinematic cuts, it is essential to consider that the signal has a clear signature with respect to the backgrounds. For the signal and the relevant backgrounds, we therefore take into account different kinematic distributions based on the cuts. Preselection is defined in the study for events with two isolated photons in the  $Z\gamma\gamma$  production and an opposite-sign same flavor dilepton in the decay of the  $Z$ -boson and this preselection is labeled with Cut-0.

According to their transverse momentum, the leading and sub-leading charged leptons ( $\ell_1$  and  $\ell_2$ ) and photons ( $\gamma_1$  and  $\gamma_2$ ) are arranged as follows:  $p_T^{\ell_1} > p_T^{\ell_2}$  and  $p_T^{\gamma_1} > p_T^{\gamma_2}$ , respectively. Fig. 3 shows the distributions of the transverse momentum of the leading charged lepton and the leading photon for the signal and the relevant background processes at the muon collider. It can be seen that the signal can be distinguished from the backgrounds by  $p_T^{\ell_1} > 50$  GeV and  $p_T^{\gamma_1} > 50$  GeV. The transverse momentum and pseudo-rapidity distributions of the leading and sub-leading charged lepton for the events are determined as  $p_T^{\ell_1} > 50$  GeV,  $p_T^{\ell_2} > 10$  GeV and  $|\eta^{\ell_{1,2}}| \leq 2.5$ , respectively, and are labeled Cut-1. However, the distributions of transverse momentum and pseudo-rapidity of the leading and sub-leading photons for the events are determined as  $p_T^{\gamma_1} > 50$  GeV,  $p_T^{\gamma_2} > 10$  GeV and  $|\eta^{\gamma_{1,2}}| \leq 2.5$ , respectively, and are labeled Cut-2.





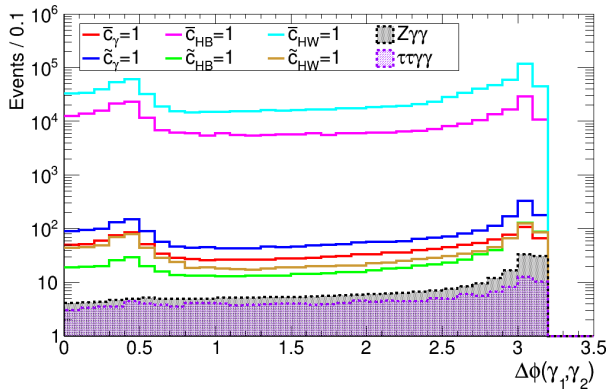
(a)



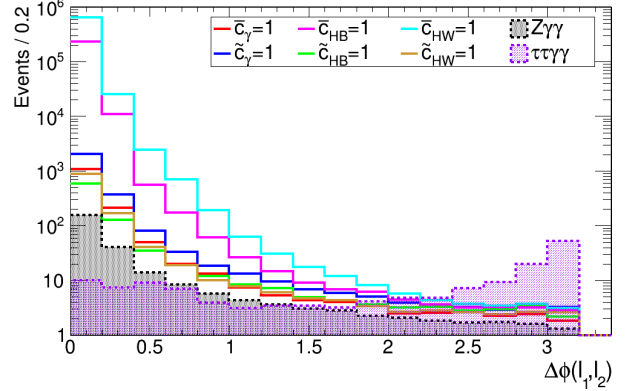
(b)

FIG. 3: The distributions of transverse momentum of the leading charged lepton (left) and the leading photon (right) for signal and relevant background processes at the muon collider.

A clear difference between signal and background is observed in the distribution of the azimuthal angle between the leading and sub-leading photons and charged leptons in Fig. 4 and in the distribution of the minimum distance between the leading and sub-leading photons and charged leptons in Fig. 5. For photons and charged leptons to be well separated in phase space leading to their identification as distinct objects in detector, kinematic cuts are needed such as  $\Delta\phi_{\gamma\gamma} < 0.8$  and  $\Delta\phi_{\ell\ell} < 1.8$  at Cut-3 and  $\Delta R_{\gamma\gamma} < 1.0$ ,  $\Delta R_{\ell\ell} < 1.4$  and  $\Delta R_{\ell\gamma} > 0.4$  at Cut-4.



(a)



(b)

FIG. 4: The distributions of azimuthal angle between the two photons (left) and two charged leptons (right) for signal and relevant background processes at the muon collider.

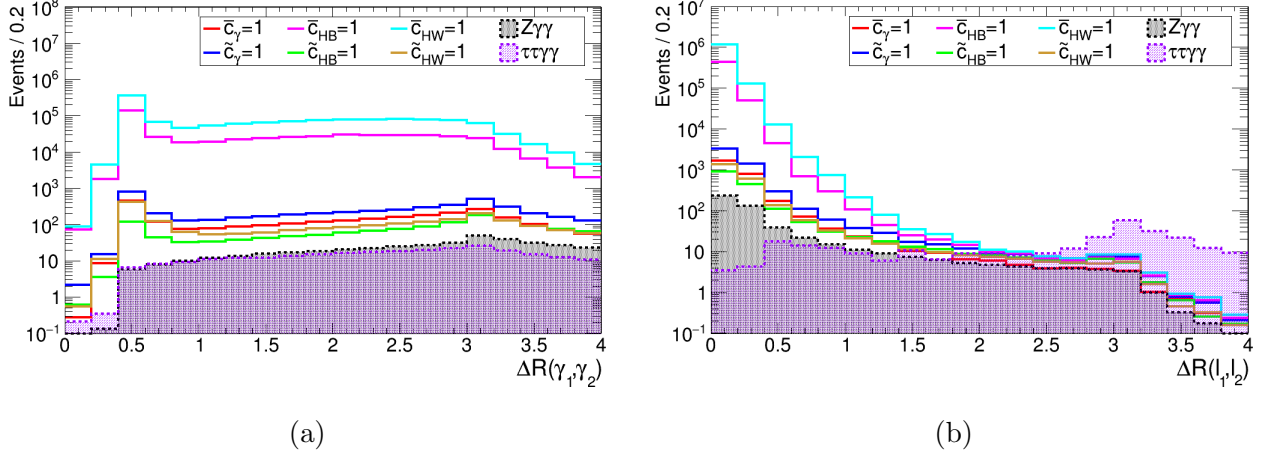


FIG. 5: The distributions of the minimum distance between the leading and sub-leading photon (left) and charged lepton (right) for signal and relevant background processes at the muon collider.

In order to separate the signal from the backgrounds in the invariant mass distribution of the photon pair and the lepton pair in Fig. 6, we set Cut-5 as  $110 \text{ GeV} < m_{\gamma\gamma} < 140 \text{ GeV}$  and  $|m_{\ell\ell} - m_Z| < 20 \text{ GeV}$ , where  $m_Z = 91.2 \text{ GeV}$ .

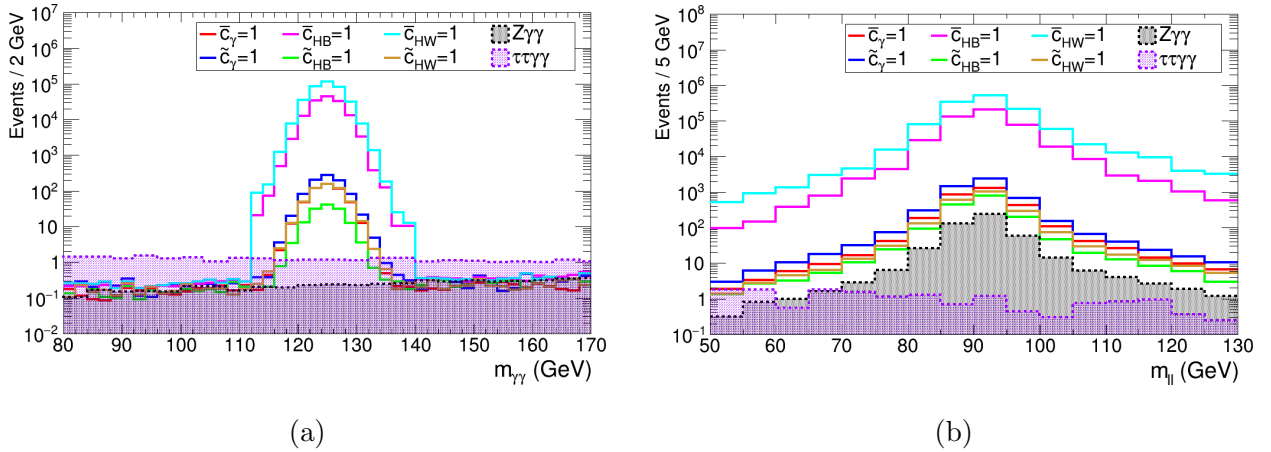


FIG. 6: The invariant mass distributions of photon pair (left) and charged lepton pair (right) for signal and relevant background processes at the muon collider.

Consequently, as illustrated in Figs. 3-6, the kinematic cuts defining deviation trends between the signal and the background and their descriptions are summarized in Table I.

TABLE I: Applied kinematic cuts in the analysis at the muon collider.

Cut flow	Definitions
Cut-0	$N_\gamma \geq 2, N_\ell \geq 2$ (least two same flavor opposite-sign leptons)
Cut-1	$p_T^{\ell_1} > 50 \text{ GeV}, p_T^{\ell_2} > 10 \text{ GeV},  \eta^{\ell_{1,2}}  < 2.5$
Cut-2	$p_T^{\tilde{\gamma}_1} > 50 \text{ GeV}, p_T^{\tilde{\gamma}_2} > 10 \text{ GeV},  \eta^{\tilde{\gamma}_{1,2}}  < 2.5$
Cut-3	$\Delta\phi_{\gamma\gamma} < 0.8, \Delta\phi_{\ell\ell} < 1.8$
Cut-4	$\Delta R_{\gamma\gamma} < 1.0, \Delta R_{\ell\ell} < 1.4, \Delta R_{\ell\gamma} > 0.4$
Cut-5	$110 \text{ GeV} < m_{\gamma\gamma} < 140 \text{ GeV},  m_{\ell\ell} - m_Z  < 20 \text{ GeV}$

The cumulative event numbers of signal ( $\bar{c}_\gamma = 1, \tilde{c}_\gamma = 1, \bar{c}_{HB} = 1, \tilde{c}_{HB} = 1, \bar{c}_{HW} = 1, \tilde{c}_{HW} = 1$ ) and relevant backgrounds ( $Z\gamma\gamma, \tau\tau\gamma\gamma$ ) after each cut used in the analysis are given in Table II. In this table, the cumulative event numbers are calculated by multiplying the cross-sections with the integrated luminosity, where the integrated luminosity of the muon collider is  $\mathcal{L}_{\text{int}} = 10 \text{ ab}^{-1}$ . The signal to total background ratio ( $S/B$ ) after each cut is presented in Table II to examine the efficiency of kinematic cuts in suppressing backgrounds. The impact of Cut-5 plays a significant role in suppressing relevant backgrounds by increasing the signal to total background ratio in cut flow by approximately 22 times.

TABLE II: The cumulative number of events for signal and relevant background processes after applied kinematic cuts at muon collider.

	Cut-0		Cut-1		Cut-2		Cut-3		Cut-4		Cut-5	
Signal	Event	$S/B$	Event	$S/B$	Event	$S/B$	Event	$S/B$	Event	$S/B$	Event	$S/B$
$\bar{c}_\gamma = 1$	193	0.95	188	1.09	184	1.16	149	1.91	94	13.8	75	300
$\tilde{c}_\gamma = 1$	429	2.11	414	2.41	403	2.55	317	4.06	194	28.4	156	624
$\bar{c}_{HB} = 1$	41218	203	38484	224	37735	239	35343	453	28834	4221	23656	94624
$\tilde{c}_{HB} = 1$	166	0.82	159	0.92	155	0.98	101	1.29	34	4.98	23	92.0
$\bar{c}_{HW} = 1$	106052	522	96585	561	95311	603	90336	1158	73853	10813	61391	245564
$\tilde{c}_{HW} = 1$	221	1.09	212	1.23	207	1.31	162	2.08	97	14.2	83	332
Background												
$Z\gamma\gamma$	70		67		65		38		4.33		0.23	
$\tau\tau\gamma\gamma$	133		105		93		40		2.50		0.02	

#### IV. SENSITIVITIES ON THE HIGGS-GAUGE BOSON COUPLINGS

The  $\chi^2$  test is used to investigate the sensitivity of Higgs-gauge boson couplings in the  $\mu^-\mu^+ \rightarrow Z\gamma\gamma \rightarrow \ell\ell\gamma\gamma$  process. The  $\chi^2$  distribution, where the critical value of  $\chi^2$  corresponding to one degree of freedom is equal to 3.84, is defined as follows in order to achieve limits at the 95% Confidence Level (C.L.):

$$\chi^2 = \sum_i^{n_{bins}} \left( \frac{N_i^{TOT} - N_i^B}{N_i^B \Delta_i} \right)^2 \quad (14)$$

where  $N_i^B$  is the number of events of relevant backgrounds and  $N_i^{TOT}$  is the total number of events including contributions of effective couplings in  $i$ th bin of the invariant mass  $m_{\ell\ell\gamma\gamma}$  distribution of  $\ell^+\ell^-\gamma\gamma$  system.  $\Delta_i = \sqrt{\frac{1}{N_i^B}}$  is the statistical uncertainty in each bin. Fig. 7 shows the invariant mass  $m_{\ell\ell\gamma\gamma}$  distribution of  $\ell^+\ell^-\gamma\gamma$  system after all applied cuts for signal and relevant background processes at the muon collider.

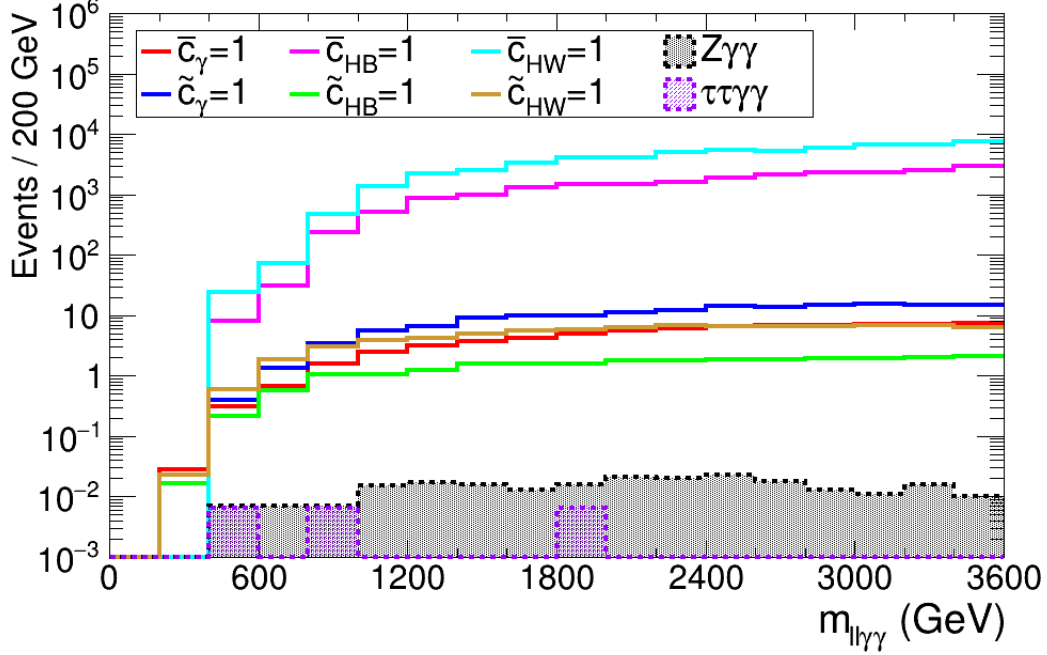


FIG. 7: The invariant mass  $m_{l\ell\gamma}$  distribution of  $l^+l^-\gamma\gamma$  final state after Cut-5 for signal and relevant background processes at the muon collider.

In Table III, the 95% C.L. limits of the coefficients  $\bar{c}_\gamma$ ,  $\bar{c}_{HB}$ ,  $\bar{c}_{HW}$ ,  $\tilde{c}_\gamma$ ,  $\tilde{c}_{HB}$  and  $\tilde{c}_{HW}$  for center-of-mass energy of 10 TeV with integrated luminosity of  $10 \text{ ab}^{-1}$  at muon collider are given and these limits are compared with the limits of experimental studies. At the muon collider, it is noticed the most sensitive limits between all coefficients belong to the coefficients  $\bar{c}_{HB}$  and  $\bar{c}_{HW}$ .

In Section II, we mentioned that the coefficients  $\bar{c}_{HB}$  and  $\bar{c}_{HW}$  make the largest contribution to the total cross-sections as a function of the Wilson coefficients and that these two coefficients are the focus of this study. Table III shows that the coefficients  $\bar{c}_{HB}$  and  $\bar{c}_{HW}$  are the most sensitive limits at the muon collider, and however, these two coefficients are even more sensitive than the experimental studies with the best limits. The limits of the coefficients  $\bar{c}_{HB}$  and  $\bar{c}_{HW}$  are discussed in detail in Section V, comparing them with the limits of experimental and phenomenological studies.

TABLE III: The 95% C.L. limits for the coefficients  $\bar{c}_\gamma$ ,  $\bar{c}_{HB}$ ,  $\bar{c}_{HW}$ ,  $\tilde{c}_\gamma$ ,  $\tilde{c}_{HB}$  and  $\tilde{c}_{HW}$  at muon collider. The limits are compared with the limits of experimental studies.

Coefficients	Muon Collider	Experimental Limits	
$\bar{c}_\gamma$	[-0.1001; 0.1216]	[-0.00074; 0.00057]	Ref. [43]
		[-0.00011; 0.00011]	Ref. [46]
$\tilde{c}_\gamma$	[-0.0862; 0.1002]	[-0.0018; 0.0018]	Ref. [43]
		[-0.00028; 0.00043]	Ref. [46]
$\bar{c}_{HB}$	[-0.0052; 0.0040]	[-0.086; 0.092]	Ref. [43]
		[-0.057; 0.051]	Ref. [44]
		[-0.022; 0.049]	Ref. [45]
$\tilde{c}_{HB}$	[-0.2241; 0.2658]	[-0.025; 0.022]	Ref. [46]
		[-0.23; 0.23]	Ref. [43]
		[-0.16; 0.16]	Ref. [44]
$\bar{c}_{HW}$	[-0.0034; 0.0023]	[-0.065; 0.063]	Ref. [46]
		[-0.086; 0.092]	Ref. [43]
		[-0.057; 0.051]	Ref. [44]
$\tilde{c}_{HW}$	[-0.1154; 0.0965]	[-0.003; 0.008]	Ref. [45]
		[-0.025; 0.022]	Ref. [46]
		[-0.23; 0.23]	Ref. [43]
		[-0.16; 0.16]	Ref. [44]
		[-0.065; 0.063]	Ref. [46]

As discussed above, when five of the six Wilson coefficients can be overly constrained, the one-parameter analysis can be beneficial in sensitivity analysis scenarios. To examine the change in the limits of the coefficients  $\bar{c}_{HB}$  and  $\bar{c}_{HW}$ , which is the focus of this study, we consider the limits where all coefficients except the coefficients  $\bar{c}_{HB}$  and  $\bar{c}_{HW}$  are set to zero. The 95% C.L. contour is obtained while  $\chi^2$ , corresponding to two degrees of freedom, is equal to 5.99 in this analysis. The 95% C.L. contour for the  $\bar{c}_{HB} - \bar{c}_{HW}$  plane at the muon collider with the two-parameter analysis is given in Fig. 8.

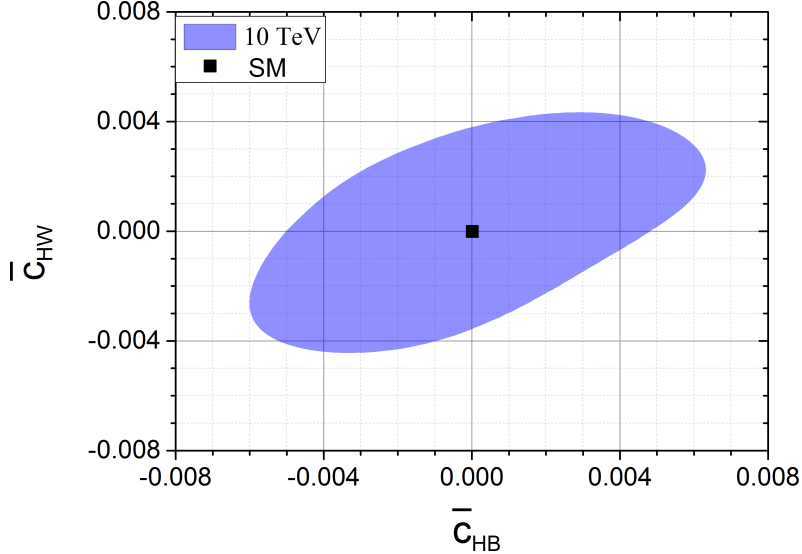


FIG. 8: Two-dimensional 95% C.L. intervals in plane for  $\bar{c}_{HB} - \bar{c}_{HW}$  at the muon collider.

## V. CONCLUSIONS

The future muon collider has recently attracted considerable attention due to its multi-TeV energy and clean environment for exploring the Higgs interactions in new physics beyond the SM. At the muon collider with a center-of-mass energy of 10 TeV and an integrated luminosity of  $10 \text{ ab}^{-1}$ , we examine the dimension-six operators of the Higgs-gauge boson couplings  $H\gamma\gamma$ ,  $H\gamma Z$  and  $HZZ$  through the process  $\mu^-\mu^+ \rightarrow Z\gamma\gamma$  using the effective Lagrangian approximation in the SILH basis. We analyze the  $\ell\ell\gamma\gamma$  production along with the decay of the  $Z$ -boson by taking into account the effects of a realistic detector with a tuned muon collider detector card. In order to separate the signal events from the backgrounds, we provide the kinematic distributions of the signal and relevant background processes in a cut-based analysis. The 95% C.L. bounds on the Wilson coefficients  $\bar{c}_\gamma$ ,  $\bar{c}_{HB}$ ,  $\bar{c}_{HW}$ ,  $\tilde{c}_\gamma$ ,  $\tilde{c}_{HB}$  and  $\tilde{c}_{HW}$  in the SILH basis are obtained using the  $\chi^2$  test from the invariant mass distribution of the  $\ell^+\ell^-\gamma\gamma$  final state.

In this study, we focus on the sensitivity of the coefficients  $\bar{c}_{HB}$  and  $\bar{c}_{HW}$  at the muon collider. The 95% C.L. bounds on the Wilson coefficients in the  $H \rightarrow \gamma\gamma$  decay channel were investigated by the ATLAS collaboration at  $\sqrt{s} = 13 \text{ TeV}$  with  $\mathcal{L}_{\text{int}} = 139 \text{ fb}^{-1}$ , and the experimental limit of the  $\bar{c}_{HB} = \bar{c}_{HW}$  coefficients was obtained as  $[-0.025; 0.022]$  [46]. In the experimental study at  $\sqrt{s} = 13 \text{ TeV}$  with  $\mathcal{L}_{\text{int}} = 79.8 \text{ fb}^{-1}$ , the ATLAS collaboration

determined the 95% C.L. bound of the coefficient  $\bar{c}_{HW}$  in the  $H \rightarrow b\bar{b}$  decay channel as  $[-0.003; 0.008]$  [45]. Comparing the limits of these experimental studies with our limits at the muon collider, the limit of the coefficient  $\bar{c}_{HB}$  is about 5 times more sensitive than in Ref. [46] and the limit of the coefficient  $\bar{c}_{HW}$  is about 2 times more sensitive than in Ref. [45].

If we consider some phenomenological studies; in Ref. [47], the 95% C.L. limits of the  $\bar{c}_{HB}$  and  $\bar{c}_{HW}$  coefficients at the CLIC with  $\sqrt{s} = 380$  GeV and  $\mathcal{L}_{\text{int}} = 500 \text{ fb}^{-1}$  are  $[-0.0482; 0.0153]$  and  $[-0.00658; 0.00555]$ , respectively, and in Ref. [48], the 95% C.L. limits of the  $\bar{c}_{HB}$  and  $\bar{c}_{HW}$  coefficients at the LHC with  $\sqrt{s} = 14$  TeV and  $\mathcal{L}_{\text{int}} = 3000 \text{ fb}^{-1}$  are  $[-0.004; 0.004]$  and  $[-0.004; 0.004]$ , respectively, in Ref. [49], the 95% C.L. limits of  $\bar{c}_{HB}$  and  $\bar{c}_{HW}$  coefficients at the LHC with  $\sqrt{s} = 13$  TeV and  $\mathcal{L}_{\text{int}} = 36.1 \text{ fb}^{-1}$  are  $[-0.230; 0.236]$  and  $[-0.236; 0.231]$ , respectively, and in Ref. [50], the 95% C.L. limits of  $\bar{c}_{HW}$  coefficient at the FCC-he with  $E_e = 60$  GeV and  $\mathcal{L}_{\text{int}} = 10 \text{ ab}^{-1}$  are found to be  $[-0.017; 0.019]$ . According to these phenomenological studies, the limit of coefficient  $\bar{c}_{HB}$  is about 7 times and 50 times more sensitive than in Ref. [47] and in Ref. [49], respectively, and almost the same order as in Ref. [48], and the limit of coefficient  $\bar{c}_{HW}$  is about 2 times, 82 times and 6 times more sensitive than in Ref. [47], in Ref. [49] and in Ref. [50], respectively, and almost the same order as in Ref. [48].

The main motivation for this study is that the clean experimental environment of the future muon collider, combined with its high center-of-mass energy and integrated luminosity, makes it a very promising option for investigating new physics beyond the SM. The more sensitive coefficients  $\bar{c}_{HB}$  and  $\bar{c}_{HW}$  for the anomalous  $H\gamma\gamma$ ,  $HZZ$  and  $H\gamma Z$  couplings at the muon collider, compared to the limits of experimental and phenomenological studies, highlight the potential of such colliders. Future muon collider experiments, together with complementary results from hadron colliders, will benefit the investigation of the fundamental nature of Higgs-gauge boson interactions. The results of this study definitely encourage further and more detailed investigations of the multi-TeV muon collider.

- 
- [1] G. Aad *et al.* [ATLAS Collaboration], *Phys. Lett. B* **716**, 1-29 (2012).
  - [2] S. Chatrchyan *et al.* [CMS Collaboration], *Phys. Lett. B* **716**, 30-61 (2012).
  - [3] G. Aad *et al.* [ATLAS Collaboration], *Eur. Phys. J. C* **76**, 658 (2016).



- [4] G. Aad *et al.* [ATLAS Collaboration], *Phys. Lett. B* **805**, 135426 (2020).
- [5] G. Aad *et al.* [ATLAS Collaboration], *Phys. Rev. Lett.* **125**, 061802 (2020).
- [6] A. M. Sirunyan *et al.* [CMS Collaboration], *Phys. Rev. Lett.* **125**, 061801 (2020).
- [7] A. Tumasyan *et al.* [CMS Collaboration], *JHEP* **06**, 012 (2022).
- [8] A. D. Sakharov, *Pisma Zh. Eksp. Teor. Fiz.* **5**, 32-35 (1967) [*Sov. Phys. Usp.* **34**, 392 (1991)].
- [9] V. A. Kuzmin, V. A. Rubakov and M. E. Shaposhnikov, *Phys. Lett. B* **155**, 36 (1985).
- [10] N. Cabibbo, *Phys. Rev. Lett.* **10**, 531 (1963).
- [11] M. Kobayashi and T. Maskawa, *Prog. Theor. Phys.* **49**, 652-657 (1973).
- [12] M. B. Gavela, P. Hernandez, J. Orloff and O. Pene, *Mod. Phys. Lett. A* **9**, 795-809 (1994).
- [13] D. E. Morrissey and M. J. Ramsey-Musolf, *New J. Phys.* **14**, 125003 (2012).
- [14] M. Chiesa, F. Maltoni, L. Mantani, B. Mele, F. Piccinini and X. Zhao, *JHEP* **09**, 098 (2020).
- [15] T. Han, W. Kilian, N. Kreher, Y. Ma, J. Reuter, T. Striegl and K. Xie, *JHEP* **12**, 162 (2021).
- [16] D. Buttazzo and P. Paradisi, *Phys. Rev. D* **104**, 075021 (2021).
- [17] T. Han, D. Liu, I. Low and X. Wang, *Phys. Rev. D* **103**, 013002 (2021).
- [18] M. Forsslund and P. Meade, *JHEP* **08**, 185 (2022).
- [19] E. Celada, T. Han, W. Kilian, N. Kreher, Y. Ma, F. Maltoni, D. Pagani, J. Reuter, T. Striegl and K. Xie, *JHEP* **08**, 021 (2024).
- [20] M. Chiesa, B. Mele and F. Piccinini, *Eur. Phys. J. C* **84**, 543 (2024).
- [21] M. E. Cassidy, Z. Dong, K. Kong, I. M. Lewis, Y. Zhang and Ya-J. Zheng, *JHEP* **05**, 176 (2024).
- [22] R. Dermisek, K. Hermanek, T. Lee, N. McGinnis and S. Yoon, *Phys. Rev. D* **109**, 095003 (2024).
- [23] S. Spor, *J. Phys. G: Nucl. Part. Phys.* **51**, 065003 (2024).
- [24] M. Forsslund and P. Meade, *JHEP* **01**, 182 (2024).
- [25] E. Gurkanli and S. Spor, “Probing CP-violating Higgs-gauge boson couplings at future muon collider,” (2024) [arXiv:2411.04565 [hep-ph]].
- [26] P. Li, Z. Liu and K.-F. Lyu, *Phys. Rev. D* **109**, 073009 (2024).
- [27] S. Spor and E. Gurkanli, “Analysis of anomalous  $H\gamma\gamma$  coupling in light-by-light collision at future muon collider,” (2024) [arXiv:2412.02346 [hep-ph]].
- [28] J. Chen, T. Li, C-T. Lu, Y. Wu and C-Y. Yao, *Phys. Rev. D* **105**, 053009 (2022).
- [29] C. Tosciri, Theoretical Introduction. *In: Higgs Boson Decays into a Pair of Bottom Quarks*,

- Springer, 2021.
- [30] G. F. Giudice, C. Grojean, A. Pomarol and R. Rattazzi, *JHEP* **06**, 045 (2007).
  - [31] A. Alloul, B. Fuks and V. Sanz, *JHEP* **04**, 110 (2014).
  - [32] J. Alwall, R. Frederix, S. Frixione, V. Hirschi, F. Maltoni, O. Mattelaer, H. S. Shao, T. Stelzer, P. Torrielli and M. Zaro, *JHEP* **07**, 079 (2014).
  - [33] A. Alloul, N. D. Christensen, C. Degrande, C. Duhr and B. Fuks, *Comput. Phys. Commun.* **185**, 2250-2300 (2014).
  - [34] C. Accettura *et al.*, *Eur. Phys. J. C* **83**, 864 (2023).
  - [35] K. M. Black *et al.*, *JINST* **19**, T02015 (2024).
  - [36] J. Chen, C-T. Lu and Y. Wu, *JHEP* **10**, 099 (2021).
  - [37] D. Buttazzo, R. Franceschini and A. Wulzer, *JHEP* **05**, 219 (2021).
  - [38] J. de Blas, J. Gu and Z. Liu, *Phys. Rev. D* **106**, 073007 (2022).
  - [39] Q.-H. Cao, K. Cheng, Y. Liu and X.-R. Wang, *Phys. Rev. D* **109**, 073005 (2024).
  - [40] C. Bierlich *et al.*, *SciPost Phys. Codebases* **8** (2022).
  - [41] J. de Favereau, C. Delaere, P. Demin, A. Giammanco, V. Lemaitre, A. Mertens and M. Selvaggi [DELPHES 3 Collaboration], *JHEP* **02**, 057 (2014).
  - [42] R. Brun and F. Rademakers, *Nucl. Instrum. Meth. A* **389**, 81 (1997).
  - [43] G. Aad *et al.* [ATLAS Collaboration], *Phys. Lett. B* **753**, 69-85 (2016).
  - [44] M. Aaboud *et al.* [ATLAS Collaboration], *Phys. Rev. D* **98**, 052005 (2018).
  - [45] M. Aaboud *et al.* [ATLAS Collaboration], *JHEP* **05**, 141 (2019).
  - [46] ATLAS Collaboration, “Measurements and interpretations of Higgs-boson fiducial cross sections in the diphoton decay channel using 139 fb<sup>-1</sup> of *pp* collision data at  $\sqrt{s} = 13$  TeV with the ATLAS detector,” ATLAS-CONF-2019-029 (2019).
  - [47] H. Denizli and A. Senol, *Adv. High Energy Phys.* **2018**, 1627051 (2018).
  - [48] C. Englert, R. Kogler, H. Schulz and M. Spannowsky, *Eur. Phys. J. C* **76**, 393 (2016).
  - [49] L. Shi, Z. Liang, B. Liu and Z. He, *Chin. Phys. C* **43**, 043001 (2019).
  - [50] H. Hesari, H. Khanpour and M. M. Najafabadi, *Phys. Rev. D* **97**, 095041 (2018).